Size dependent of refractive index changes of $GaN/Al_xGa_{1-x}N$ core-shell quantum dots with and without a donor impurity

A. ELKADADRA, D. ABOUELAOUALIM*, A. OUERIAGLI, A. OUTZOURHIT
LPSCM, Department of Physics, Faculty of Sciences Semlalia, Cadi Ayaad University P.O. Box 2390, 40000 Marrakech, Morocco

In thisstudy, the total refractive index (RI) changes of GaN / $Al_xGa_{1-x}N$ Core-Shell quantum dots are calculated with a hydrogenic impurity. Our results show that the RI changes are considerably sensitive to the geometrical parameters of systems. The peak position of the total refractive index changes is greatly affected by changing of the geometrical size and presence of the hydrogenic impurity. The possibility of tuning the resonant energies by using the geometric core shell effect of the spatial confinement can be useful in the optoelectronic devices applications.

(Received September 5, 2013; accepted May 15, 2014)

Keywords: Core-Shell, Quantum dot, Refractive index changes

1. Introduction

Quantum confinement (QC) leads to formation of an ordered set of orbitals at discrete energy levels on the conductionand valance bands in semiconductor quantum dots (QDs) [1-4], which enables strongly size-dependent control of opticalproperties. Especially when the physical size of a QD is comparable to or smaller than the exciton in its bulk semiconductormaterial, QC modifies strongly the electronic structure.

Recently, in order to aim of improving the electronic structures and optical properties of QDs structure singlephoton detector for application as an optical data storagemedium, different shapes and various confinement potentials have been widely studied. Core shell quantum dot (CSQD) [5-8] containing shells have been investigated to seek superior structural properties allowing for strain reduced band engineering. The linear and nonlinear optical properties of these structures are very attractive for scientists both experimentallyand theoretically [9-13].In this regard, we consider a $GaN/Al_xGa_{1-x}N$ spherical core-shell quantum dots (CSQD) with a finite confining potential height, and investigate the effects of the sizeof core-shell on refractive index (RI) changes with and without impurity.

This paper is organized as follows: In the next section, details of the calculations are presented. Results and discussions are given in Sec. III. A brief conclusion is presented in Sec. IV.

2. Model and theory

The model used in calculation and analyses is an isolated $GaN/Al_xGa_{1-x}N$ core-shell quantum dot with core radius R1 and shell radius R2, shown in Fig. 1.

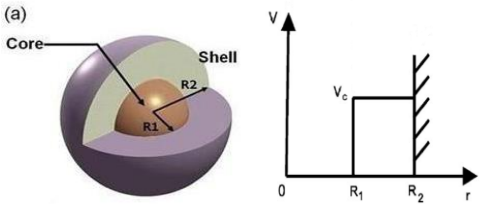

Fig. 1. Core-shell GaN-$Al_xGa_{1-X}N$ quantum dot system showing (a) core and shell layers; and (b) layer potential profile.

Suppose the core-shell quantum dot forms a shell well and a centric barrier for the two kinds of materials have different potentials. The potential of the core is chosen to be referent zero point of energy, and the band-gap of GaN is wider than that of $Al_xGa_{1-x}N$, thus V_C.On the premise of the effective mass approximation, the steady Schrödinger equation for electron can be written as

$$\left\{-\frac{\hbar^2}{2m_i^* r^2}\left[\frac{\partial}{\partial r}\left(r^2\frac{\partial}{\partial r}\right)+\frac{1}{\sin\theta}\frac{\partial}{\partial\theta}\left(\sin\theta\frac{\partial}{\partial\theta}\right)+\frac{1}{\sin^2\theta}\frac{\partial^2}{\partial\varphi^2}\right]+V_i(r)\right\}=E\,\Phi_{nlm}(r), \quad (1)$$

where, $\hbar$=h/2π , h is Planck's constant; E the energy eigenvalue; and $\Phi_{nlm}(r)$ the responding eigenfunction. n is the principal quantum number, and l and m are the angular momentum quantum numbers. m_i^* is the effective mass of electron in the ith region, $\varepsilon(r)$ constant of core /shell QDs materials and $V_i(r)$ the potential. They are relative to the position in the model and expressed as follows

$$m_i^* = \begin{cases} m_1^* & r \le R_1, \\ m_2^* & R_1 < r \le R_2 \end{cases} \tag{2}$$

$$V_i(r) = \begin{cases} 0, & 0<\mathrm{r} \le R_1, \\ V_{c,} & R_1<\mathrm{r} \le R_2, \\ \infty, & \mathrm{r}\rangle R_{2,} \end{cases} \tag{3}$$

Due to the fact that the mass and the potential are symmetric spherically, the separation of radial and angular coordinates leads to $\Phi_{nlm}(r) = R_{nlm}(r) Y_{nlm}(\theta,\varphi)$, where $R_{nlm}(r)$ is the radial wave function, and $Y_{nlm}(\theta,\varphi)$ is the spherical harmonics. The radial eigenfunction, $R_{nl}(r)$ consists of three parts according to the electron position. Two cases need to be considered for the solution of $R_nl(r)$. In regions where electron eigenenergy $E \langle V_c$, the solution is a linear combination of spherical Bessel function *jl* and Neumann function *nl*, written as

$$R_{nl}(r) = \begin{cases} A_1 J_l\left(k_{nl,1} r\right) + B_1 n_l\left(k_{nl,1} r\right), & r \le R_{1,} \\ A_2 J_l\left(k_{nl,2} r\right) + B_2 n_l\left(k_{nl,2} r\right), & R_1 \langle r \le R_{2,} \\ 0, & r\rangle R_{2,} \end{cases} \tag{4}$$

with

$$k_{nl,2} = \sqrt{2m_1^* E/\hbar^2}, \tag{5}$$

$$k_{nl,2} = \sqrt{2m_2^* (V_c - E)/\hbar^2}, \tag{6}$$

A_1, A_2, B_1, and B_2 are normalized constants . In regions where $E \rangle V_c$, the radial wave function is

$$R_{nl}(r) = \begin{cases} A_1' J_l\left(k_{nl,1} r\right) + B_1' J_l\left(k_{nl,1} r\right), & r \le R_{1,} \\ A_2' h_l^{(+)}\left(k_{nl,2} r\right), & R_1 \langle r \le R_{2,} \\ 0, & r\rangle R \end{cases} \tag{7}$$

With A_1', A_2', and B_1' are normalized constants.

Let us consider that the system is excited by a monochromatic electromagnetic field, $E(t) = Ee^{i\omega t} + c.c.$, which is polarized along the Z-direction. Therefore, the time evolution of the density operator of the system is given by [13]

$$\frac{\partial \tilde{\rho}}{\partial t} = \frac{1}{i\hbar}\left[\hat{H} - \hat{M}E(t), \rho\right] - \hat{\Gamma}\left(\hat{\rho} - \hat{\rho}^0\right), \tag{8}$$

where H is the Hamiltonian of the system in the absence of the electromagnetic field, $\hat{M} = e\hat{z}$ is the dipole operator along the Z-axis, $\hat{\rho}^0$ is the unperturbed density operator and Γ is the damping operator due to the electron-phonon interaction and the other collision processes. The above equation can be solved using the perturbation method by expanding ρ as [13]

$$\tilde{\rho} = \sum_n \tilde{\rho}^{(n)} \tag{9}$$

$$\frac{\partial \rho_{ij}^{(n+1)}}{\partial t} = \frac{1}{i\hbar}\left\{\left[\tilde{H}, \tilde{\rho}^{(n+1)}\right]_{ij} - \left[\tilde{M}, \tilde{\rho}(n)\right]_{ij} E(t) - i\hbar\Gamma_{ij}\partial\tilde{\rho}^{(n+1)}\right\}, \tag{10}$$

On the other hand, the electric polarization of the system can be written as

$$\begin{aligned} P(t) &= \varepsilon_0 \chi(\omega) E e^{-i\omega t} + \varepsilon_0 \chi(-\omega) E e^{i\omega t} \\ &= \frac{1}{V} trace\left(\tilde{\rho}\tilde{M}\right), \end{aligned} \tag{11}$$

Where V is the volume of the system, ε_0 is the permittivity of free space, and trace means the summation over the diagonal elements of the matrix. Using the same density matrix formalism, the analytic expressions of the linear and the third order nonlinear susceptibilities for a two-level quantum system are given and ε' is the real part of the permittivity [14]:

$$\varepsilon_0 \chi^{(3)}(\omega) = \frac{\sigma_v |M_{ij}|^2 |E|^2}{E_{ij} - \hbar\omega - i\hbar\Gamma_{ij}} \left[\frac{4|M_{ij}|^2}{\left(E_{ij} - \hbar\omega\right)^2 + \left(\hbar\Gamma_{ij}\right)^2} - \frac{\left(M_{ff} - M_{jj}\right)^2}{\left(E_{fj} - i\hbar\Gamma_{if}\right)\left(E_{fj} - \hbar\omega - i\hbar\Gamma_{if}\right)}, \right. \tag{12}$$

$$\varepsilon_0 \chi^{(1)}(\omega) = \frac{\sigma_v |M_{ij}|^2}{E_{ij} - \hbar\omega - i\hbar\Gamma_{ij}} \tag{13}$$

where σ_v is the carrier density, $E_{fj} = E_f - E_i$ is the energy interval of the two level system. M_{fj} is the dipole matrix

element, which is defined by $M_{fi} = |\langle \Psi_f | er | \Psi_i \rangle|$, $(f, i = 1,2)$ and Γ shows the damping due to electron-phonon interaction. The refractive index is given by

$$\Delta n = \frac{1}{2n_r \varepsilon_0} \mathrm{Re}(\varepsilon_0 \chi(\omega)) \tag{14}$$

or

$$n_r = \mathrm{Re}(\sqrt{1+\chi(\omega)}) \approx 1 + \frac{1}{2}\mathrm{Re}(\chi) \tag{15}$$

The total refractive index changes can be written as

$$\frac{\Delta n}{n_r} = \frac{1}{2n_r^2 \varepsilon_0} \mathrm{Re}(\varepsilon_0 \chi(\omega)) \tag{16}$$

Let us consider a CSQD containing hydrogen like impurity. Moreover, it assumedthat the impurity is located in core. As the previous case, confining potential is chosen in the form (1). Taking intoaccount the Coulomb field the Hamiltonian of the systemhas the form In the case of a hydrogenic impurity in the center of symmetry of a coreshell quantum dot, the Hamiltonian of Eq.(1) is modified tobe

$$H = H_0 - \frac{e^2}{\varepsilon r} \tag{17}$$

3. Numerical results and analysis

In the numerical calculations carried out for a core-shell quantum dot, the following parameter values have been used [15]: characterize the electrical and optical properties of the physical parameters used in our numerical work for GaN and $Al_xGa_{1-x}N$ are taken from ref [8]. The effective mass is $m^*_{GaN} = 0.19 m_e$ $m^*_{Al_xGa_{1-x}N} = \left(0.19(1-x) + 0.33\right) m_0$. The band-gap is $\Delta E_c = x\,6.13eV + (1-x)3.42eV - x(1-x)1.0eV$.

The conduction band offset is chosen as $V_c = 0.75\left(E_g(x) - E_g(0)\right)$. The dephasing constant corresponding to elastic scattering is $\Gamma_{13} = 0.14ps$ and the incident optical intensity is $I = 1MW/\mathrm{cm}^3$.

In Fig. 2, the total optical RI as a function of the incident photon energy have been plotted for a spherical CSQD with three different core radii R_1,

R_2=62 A, and x=0.15. As we can see from Fig. 2, that as the dot radius R_1 increases, the RI change peak positions will move to the left side, which show a dot-radius-induced red shift of the resonance in a spherical CSQD. The peak value of the RI is a monotonic function of the dot radius R_1.

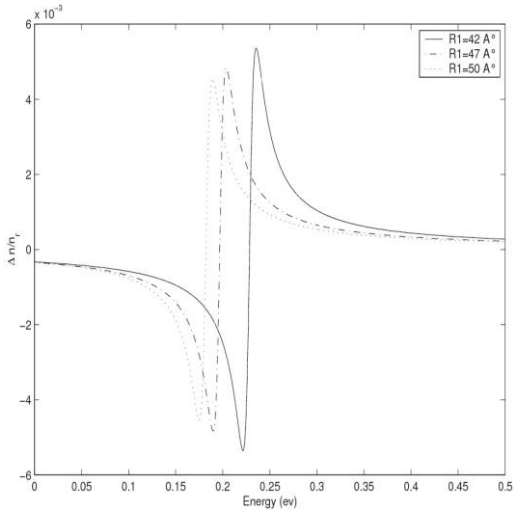

Fig. 2. The total RI of CSQD without donor impurity, as a function of incident photon energy with the fixed shell radii R2 = 62 A° for different values of core radii R_1.

The physical origin is that when the dot radius decreases, on the one hand, the CSQD size will decrease so that the overlapping of the wave functions of the ground and the first excited states increases, on the other hand, the wave functions will overflow because of the finite barrier height.

In Fig. 3, the total optical RI as a function of the incident photon energy have been plotted for a spherical QD with three different dot radii R_2, R_1=48A°, and x=0.15.

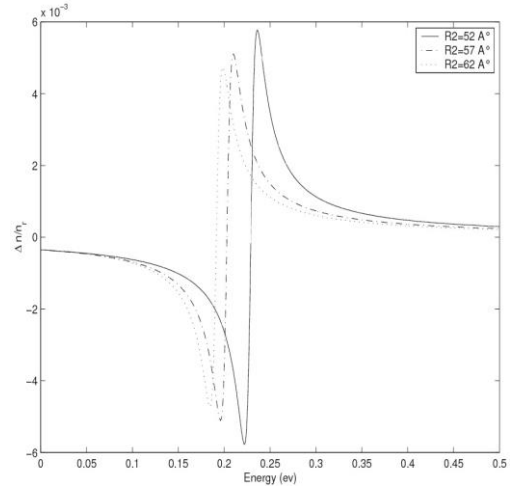

Fig. 3. The total RI of CSQD without donor impurity, as a function of incident photon energy with the fixed shell radii R_1 = 48 A° for different values of core radii R_2.

As we can see from Fig. 3, that when the dot radius R_2 increases, the RI change peak positions will move to the left side, which show a dot-radius-induced red shift of the resonance in a CSQD. The peak value of the RI is a monotonic function of the dot radius R_2. The physical origin is that when the dot radius decreases, on the one hand, the CSQD sizes will decreases so that the

overlapping of the wave functions of the ground and the first excited states increases, on the other hand, the wave functions will overflow because of the finite barrier height.

In Fig. 4, and Fig. 5, the Al concentration is set to 0.15, and the position of the impurity is the center of CSQD. In Fig. 4, we have shown the total refractive index changes as a function of the photon energy for three different shell radius R1values, with the fixed shell radii R_2 = 62 A°.

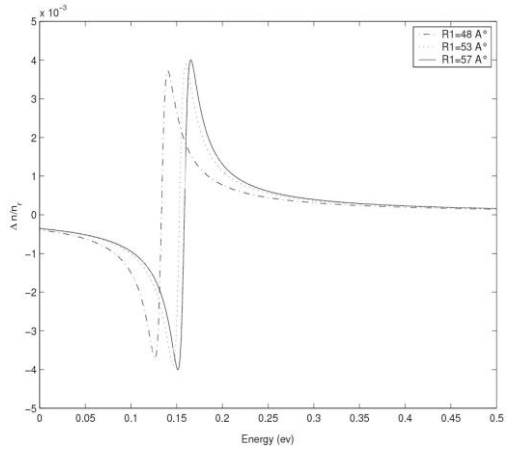

Fig. 4. The total RI of CSQD with donor impurity in center, as a function of incident photon energy with the fixed shell radii R_2 = 62 A° for different values of core radii R_1.

As it can be seen from the curves, the total RI peak has significant shift and the height of total RI peak enhanced when core radius increases. The physical origin of these results is that the CSQD radius has obvious effects on the transition matrix element and also the electron density in CSQDs which is related to the total AC.

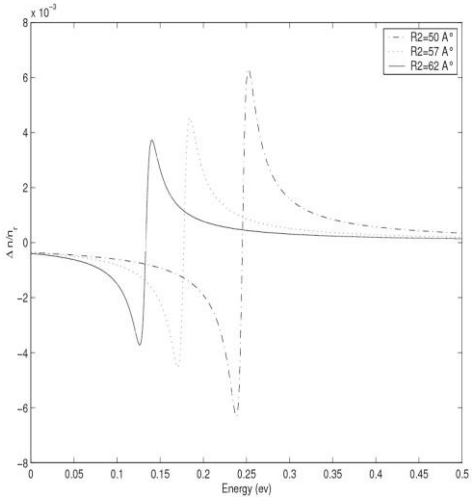

Fig. 5. The total RI of CSQD with donor impurity in center, as a function of incident photon energy with the fixed shell radii R2 = 48 A° for different values of core radii R_2.

Finally, in Fig. 5, we display the total RI as a function of the incident photon energy for three different shell radius R2 values. It is clear that as R2 increases, the RI increase and also shift toward higher energies until it reaches a maximum value.

4. Conclusions

We have investigated the refractive index changes in a GaN / AlxGa1-x N core shell quantum dot. We have found that the geometrical parameters (size) core shell quantum dot have a significantly influence on the total optical RI, and the peaks shift toward the highest energies as R1 (R2) decreases with donor impurity in center.

We expect that this work will be of great help for describing the correct behavior of optical properties in CSQD with different size, which may be useful in technological applications as water purification, high density optical storage.

References

[1] Mehmet Şahin, J. Appl. Phys. **106**, 063710 (2009).
[2] J. Salfi, S. Roddaro, D. Ercolani, L. Sorba, I. Savelyev, M. Blumin, H. E. Ruda, F. Beltram, Semicond. Sci. Technol. **25**, 024007 (2010).
[3] Ł. Kłopotowski, Ł. Cywiński, M. Szymura, V. Voliotis, R. Grousson, P. Wojnar, K. Fronc, T. Kazimierczuk, A. Golnik, G. Karczewski, T. Wojtowicz, Phys. Rev. **B87**, 245316 (2013).
[4] E. A. Chekhovich M. N. Makhonin A. I. Tartakovskii A. Yacoby H. Bluhm K. C. Nowack, L. M. K. Vandersypen, Nature Materials **12**, 494 (2013).
[5] Jens U. Sutter, David J. S. Birch, Olaf J. Rolinski, Meas. Sci. Technol. **23**, 055103 (2012).
[6] Soon Il Jung, Ilgu Yun, Il Ki Han, Sung M. Cho, Joo In Lee, J. Korean Phys. Soc, **52**(6), 1891 (2008).
[7] Guozhi Jia, Bingxue Hao, Xucen Lu, Jianghong Yao, Int. J. Electrochem. Sci., **8**, 8167 (2013).
[8] W. K. Bae, L. A. Padilha, Y. S. Park, H. McDaniel, I. Robel, J. M. Pietryga, V. I. Klimov, ACS Nano; **7**(4), 3411 (2013).
[9] R. A. M. Hikmet, D. V. Talapin, H. Weller, J Appl. Phys. **93**, 3509 (2003).
[10] L. Manna, D. J. Milliron, A. Meisel, E. C. Scher, A. P. Alivisatos, Nat Mater. **2**, 382 (2003).
[11] A. J. Nozik, M. C. Beard, J. M. Luther, M. Law, R. J. Ellingson, J. C. Johnson, Chem. Rev. **110**, 6873 (2010).
[12] Y. Xing, X. X. Liang, Z. P. Wang, Mod. Phys. Lett. B **27**, 1350134 (2013).
[13] A. Mmadi, K. Rahmani, I. Zorkani, A. Jorio, Superlattices and Microstructures **57**, 27 (2013).
[14] K. G. Devoyan, E. M. Kazaryan, L. S. Petrosyan, Physica E **28**, 333 (2005).
[15] I. Karabulut, S. Baskoutas, J. Appl. Phys. **103**, 073512 (2008).
[16] Wu Feng, Zhang Guilan, Tian Wei, LinaChen, Wenju, Zhao Guofeng, Cao Shidong Xie, Wei, J .Opt A: Pure Appl. Optics, **10**(7), 75103 (2008).

*Corresponding author: d.abouelaoualim@uca.ma